A Sub-Wavelength RF Source Tracking System for GPS-Denied Environments

Fikadu T. Dagefu, *Student Member, IEEE*, Jungsuek Oh, *Student Member, IEEE*, and Kamal Sarabandi, *Fellow, IEEE*

***Abstract*—A sub-wavelength source tracking system utilizing highly miniaturized antennas in the HF range for applications in GPS-denied environments including indoor and urban scenarios is proposed. A technique that combines a high resolution direction finding and radio triangulation utilizing a compact transmit (Tx) and receive (Rx) antenna system is pursued. Numerical models are used to investigate wave propagation and scattering in complex indoor scenarios as a function of frequency. We choose HF band to minimize attenuation through walls and multipath in indoor environments. In order to achieve a compact system, a low-profile and highly miniaturized antenna ($\lambda/300$ height and $\lambda/100$ lateral dimensions at 20 MHz) having omnidirectional, vertically polarized field is designed. At such low frequencies, accurate measurement of the phase difference between the signals at the Rx antennas having very small baseline is challenging. To address this issue, a biomimetic circuit that mimics the hearing mechanism of a fly (Ormia Ochracea) is utilized. With this circuit, very small phase differences are amplified to measurable values. The numerical simulations are used to analyze direction of arrival retrieval and source localization in highly cluttered environments. A compact system prototype is also realized and source tracking in complex indoor scenarios is successfully demonstrated.**

***Index Terms*—GPS-denied environments, RF indoor source tracking.**

I. Introduction

THE ability to accurately detect the direction of arrival and track the location of a source in complex and GPS-denied environments is useful for a wide variety of applications such as fire and earthquake rescue missions, user position estimation in mobile communications and for security systems. Another application of interest pertains to real time positioning and tracking of robotic platforms that are used to enhance tactical situational awareness in complex environments including urban and indoor scenarios. A specific example of this is assisting the aforementioned platform in high-resolution navigation in these cluttered environments. Available techniques for direction finding that are based on time-of-arrival (TOA), time-difference-of-arrival (TDOA) and received signal strength indicator (RSSI) often involve complex algorithms [1]–[6]. TOA and TDOA based approaches also have an inherent issue associated with clock drift [6]. Angle of arrival (AOA)-based methods are relatively simple (with some complexity related to antenna calibration) and can be reliably used to determine the direction of a source [7], [8]. Hybrid approaches that combine AOA and TDOA techniques have also been reported [9] and [10]. In GPS-denied environments such as indoor and urban scenarios, the task of localizing and tracking an RF source is even more challenging because of multipath. The level of multipath increases significantly at frequencies utilized in conventional wireless systems (2–5 GHz range) or even in the VHF range compared to the HF band [11], [12]. Given a Tx and Rx antenna system located in a cluttered environment as depicted in Fig. 1, the signal at the Rx antenna consists of the direct, reflected, diffracted and multiply scattered components from the objects within the environment. The path lengths of multiply scattered fields can be quite different from other field components (direct). A full-wave analysis of multipath levels in indoor scenarios is presented in Section III. Several researchers have worked on ultrawideband (UWB) systems and different signal processing algorithms for non-line-of-sight (NLOS) source localization [13]–[16]. Other approaches include vision-based position estimation and tracking based on sensors integrated in the environment itself [17], [18].

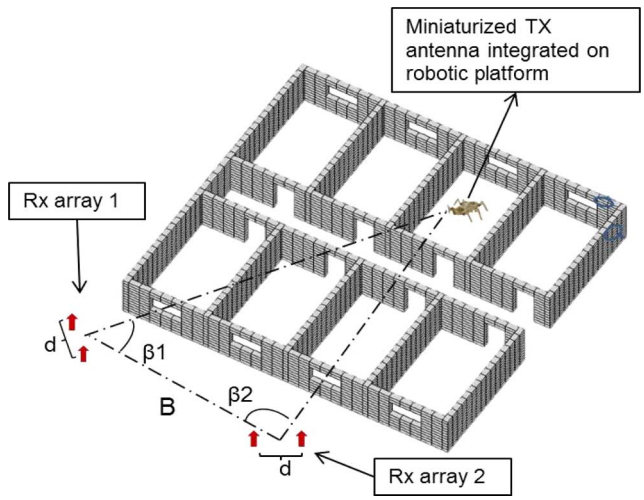

Fig. 1. Schematic illustrating the proposed approach. It consists of a complex building scenario, receiver arrays, and the Tx antenna (building picture is borrowed from [21]).

In this paper, a source tracking technique based on a combination of radio triangulation and a direction retrieval approach utilizing a compact Rx antenna array in the HF range is proposed. The system consists of a highly miniaturized Tx antenna and a Rx array whose inter-element spacing is only a fraction of the wavelength. The advantage of choosing the operating frequency

Manuscript received April 18, 2012; revised November 16, 2012; accepted November 21, 2012. Date of publication December 05, 2012; date of current version April 03, 2013. This work was supported by the U.S. Army Research Laboratory under contract W911NF and prepared through collaborative participation in the Microelectronics Center of Micro Autonomous Systems and Technology (MAST) Collaborative Technology Alliance (CTA).

The authors are with the Radiation Laboratory, Department of Electrical Engineering and Computer Science, The University of Michigan, Ann Arbor, MI 48109 USA (e-mail: fikadu@umich.edu; jungsuek; saraband@umich.edu).

Color versions of one or more of the figures in this paper are available online at http://ieeexplore.ieee.org.

Digital Object Identifier 10.1109/TAP.2012.2232036

0018-926X/$31.00 © 2012 IEEE

Authorized licensed use limited to: Seoul National University. Downloaded on December 15,2022 at 13:59:12 UTC from IEEE Xplore. Restrictions apply.

in the HF band is two-fold. First, scattering from walls ceiling and furniture will be small compared to the direct path making direction finding with only a small error possible. The second advantage of using HF is that wave propagation for near-ground antennas where the Tx and Rx antenna heights are less than a wavelength (λ) is supported by Norton surface waves which attenuate as $(1)/(R^2)$ where R is the distance between the Tx and Rx antenna, hence further reduces the effect of multipath from walls [19]. That is, the dominant component of the received signal is the direct path between the receiver and the transmitter. Numerical models are utilized to investigate wave propagation and scattering in complex indoor scenarios and to determine the highest frequency at which the required tracking resolution can be achieved in the presence of the scatterers. One disadvantage of using low frequencies is that the size of the antenna becomes prohibitively large especially for applications that require a compact system. So, one challenge is to design a compact antenna to be used both for the Tx and Rx antennas. For our system prototype, we designed a miniaturized antenna having vertical polarization and an omnidirectional radiation pattern. In the presence of the ground only, the received signal is maximized when both the Tx and Rx antennas are vertically polarized (VV polarization). Another challenge that is addressed in this paper has to do with the small antenna spacing of the receive array. At low frequencies such as the HF range, the phase difference between the received signals, which is an important quantity of interest, becomes too small to be measured. To tackle this issue, a phase difference amplification scheme that mimics the hearing mechanism of a fly (Ormia Ochracea) is designed and fabricated. The system validation and resolution analysis based on numerical and measurement results is discussed.

The rest of the paper is organized as follows. In Section II, we describe the proposed source tracking technique. In Section III, numerical techniques are utilized to investigate wave propagation in realistic indoor scenarios and to analyze the performance of the proposed approach. The effect of antenna coupling between closely spaced Rx antennas is also analyzed using full-wave simulation. In Section IV, we describe the system prototype along with the design and test results of various components including the phase difference amplification circuit. Also in this section, a description of a low-profile highly miniaturized antenna used in the system prototype is included. The approach utilized to achieve impedance matching and omnidirectional radiation pattern is described. We then discuss the source tracking system test results for various multipath environments.

II. Proposed Source Tracking Approach

The technique we are proposing for direction finding utilizes the received signals on an array of antennas closely positioned ($\lambda/15$ spacing) on a rotating platform. A schematic showing the proposed technique is given in Fig. 1. The magnitude and phase differences between the received fields on the elements of the array provide information about the direction of the source. The direction of arrival (DOA) is determined using the phase and magnitude of the received signals based on

$$\mathrm{DOA} = \underset{\theta_i}{\mathrm{Min}} \left[\left| \Phi\left(E_1^r(\theta_i)\right) - \Phi\left(E_2^r(\theta_i)\right) \right| \right] \tag{1}$$

$$\mathrm{DOA} = \underset{\theta_i}{\mathrm{Min}} \left[\frac{\left| E_1^r(\theta_i) - E_2^r(\theta_i) \right|}{\left| E_1^r(\theta_i) + E_2^r(\theta_i) \right|} \right] \tag{2}$$

where $E_1^r(\theta_i)$ and $E_2^r(\theta_i)$ are the complex received fields at each element of the receive array as a function of the incidence angle θ_i (the angle between the bisect of the Rx array and the incident wave) and Φ which is the phase of the received field. The DOA of a given source needs to be correctly retrieved from at least two locations separated by a known baseline outside the building. By using the coordinates of the receiver arrays and the retrieved angles (β_1 and β_2), the location of the source is calculated by triangulation. The vector baseline $\vec{B}$ can be characterized very accurately, for example, using a differential GPS unit mounted on the two platforms. As it was alluded to in the previous Section, to minimize the effect of multipath as much as possible, the use of the lower band of the electromagnetic spectrum (HF-band) is proposed. When the level of multipath increases (i.e., when the frequency of operation for a given geometry of propagation scenario is increased), the resolution of the retrieved DOA will degrade. It is shown that based on full-wave simulations in the presence of mostly dielectric scatterers, the direction finder works with good resolution in the HF range. Another advantage of using HF has to do with near-ground propagation effects which is unique to antennas that are very close to the ground in terms of wavelength. The Tx and Rx antenna heights for many of the applications of interest is only a small fraction of the wavelength. For example, at 20 MHz, 1-m antenna height is only $\lambda/15$. Wave propagation at such low antenna heights is dominated by Norton surface waves [19], [20]. For near-ground antennas, unlike in the case of antennas that are well removed from the ground (having heights greater than a wavelength), the received electric field which is dominated by Norton surface waves decay as $(1)/(R^2)$ [19]. For this reason, in the presence additional scatterers, multipath effects also decay fast for near-ground antennas.

In order to achieve a high-resolution source tracking system, there are three things that need to be considered. First, the signal-to-noise ratio (SNR) should be maximized because it is the main limiting factor determining the smallest phase difference that can be accurately measured which in turn determines the maximum tracking resolution. Secondly, the orientations for each antenna should be selected so that the received signal is maximized while the multipath effects are further minimized. In the proposed system vertically polarized transmit and receive antenna arrays are chosen to maximize the received signal. The third important variable is the spacing between the antenna elements in two Rx antenna array sets as it has to be large enough so that the phase difference due to path length differences is not too small.

III. Propagation Modeling and Analysis

For Tx and Rx antennas located in a complex propagation environment, the received signal includes the direct, reflected, diffracted and multiply scattered components from the scatterers in the environment. The major scatterers in indoor environments are walls, big furniture, ceilings and the ground. In order to quantify the effect of multipath on the DOA retrieval technique,

Authorized licensed use limited to: Seoul National University. Downloaded on December 15,2022 at 13:59:12 UTC from IEEE Xplore. Restrictions apply.

TABLE I
WALL REFLECTIVITY (TW IS THICKNESS OF THE WALL, $\epsilon_r' = 4$ AND $\epsilon_r'' = 3.6$@ 5 MHz), ϕ_i IS THE INCIDENT ANGLE MEASURED FROM THE NORMAL TO THE INTERFACE

f [MHz]	Tw [cm]	$\lvert\Gamma_{TE}\rvert$ $\phi_i = 30°$	$\lvert\Gamma_{TM}\rvert$ $\phi_i = 30°$	$\lvert\Gamma_{TE}\rvert$ $\phi_i = 60°$	$\lvert\Gamma_{TM}\rvert$ $\phi_i = 60°$
5	15	0.04	0.03	0.07	0.01
20	15	0.11	0.08	0.18	0.02
5	25	0.07	0.05	0.11	0.02
20	25	0.18	0.12	0.29	0.03
100	25	0.59	0.45	0.78	0.08

an accurate and efficient propagation model that takes into account scattering from the major indoor scatterers is required. Once we have a propagation model, we can then quantify the effects of indoor scatterers as a function of frequency, geometry of the problem, and electromagnetic properties of the various scatterers. As a first-order analysis to investigate the effects of walls and similar scatterers, we will first calculate the reflection coefficient from a single dielectric wall for different values of wall thicknesses, incidence angles and frequencies. Here, the wall is essentially modeled as a dielectric slab having an effective complex dielectric constant. The real (ϵ_r') and imaginary part (ϵ_r'') of the dielectric constant of the wall used for this calculation are 4 and 0.9 at 20 MHz, respectively. At 100 MHz, ϵ_r' is 4 and ϵ_r'' is 0.2. The use of a constant effective dielectric constant for the walls is a good approximation for realistic walls made out of bricks or cinderblocks at the frequency of interest (HF band).

Table I shows the wall reflectivity values, Γ_{TE} and Γ_{TM}, for transverse electric and transverse magnetic components of the incident wave. These results show that only a small fraction of the signal is reflected by the wall (especially in the HF band). For example, about 80% of the incident field is transmitted through the wall at 20 MHz independent of incidence angle for concrete walls as thick as 25 cm. It can be seen that reflection coefficient significantly increases with frequency. The main point of this analysis is to show that the HF band is desired for source tracking in indoor settings, since at this frequency the multipath becomes much less significant than at higher frequencies. In the rest of this section, we present full-wave simulation results of a typical complex indoor propagation scenario to quantitatively investigate and justify the choice of HF band for source tracking in cluttered environments.

A. Full-Wave Simulation in the Presence of Dielectric and Metallic Scatterers

In order to study the effect of multipath using a more realistic model, we used a second model based on a finite-difference time-domain (FDTD) full-wave solver. The full-wave simulation is important because it takes into account near-ground wave propagation and antenna coupling effects that ray tracing does not consider. We will consider the setup given in Fig. 2 which will be used to investigate the level of multipath as a function of frequency using field coverage comparison. The performance of the proposed tracking technique will also be analyzed. The geometry used for this simulation is a complex building setting consisting of several walls and the ground. The walls and the ceiling are modeled as dielectric slabs. The dielectric properties of the walls are chosen to be that of cinder block

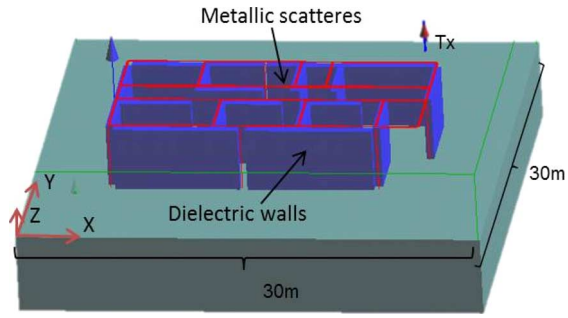

Fig. 2. Full-wave simulation setup to investigate field coverage as a function of frequency is shown. Several steel cylinders are included as support for the dielectric walls and the ceiling (similar to realistic buildings). The dielectric ceiling is not shown in this picture. A short dipole located outside is utilized as a Tx antenna and field coverage inside and outside the building is analyzed.

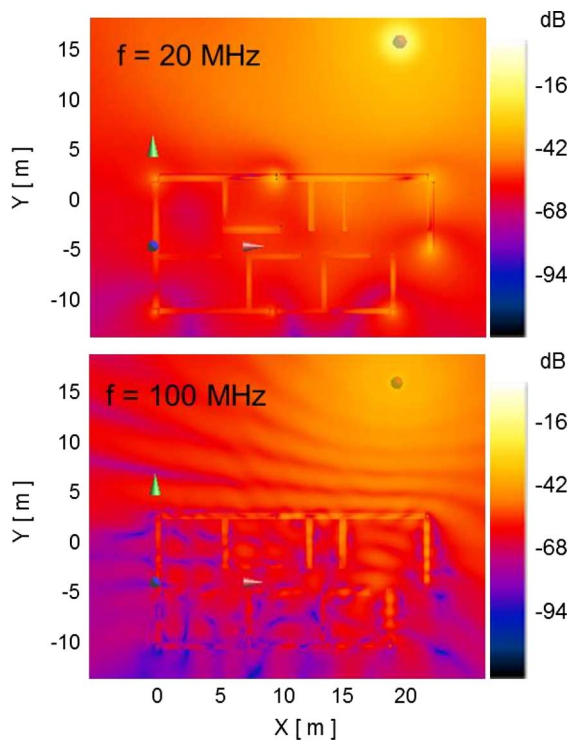

Fig. 3. Comparison of magnitude of the vertical component of the electric field coverage as a function of frequency on a plane parallel to the ground (at a height of $z_o = 1.5$ m for the setup given in Fig. 2.

$(\epsilon_r = 4 + 0.9j)$. The ground is modeled as a concrete half-space medium. The dielectric constant of concrete in the HF range is assumed to be $\epsilon_r = 4.5 + 0.9j$. To make the environment more realistic, a metallic frame is considered as support for the dielectric walls and ceiling (Fig. 2, dielectric part of the ceiling is not shown). A z-directed short dipole located outside the building is utilized as a Tx antenna and the electric field coverage is computed as a function of frequency. It should be noted that absorbing boundary conditions have to be correctly placed to avoid diffracted components from the edges of the ground. For this reason perfectly matched layer (PML) boundary conditions without any air padding are utilized to simulate infinite ground.

The vertical component of the electric field on a plane parallel to the ground at a height $z_o = 1.5$ m is plotted for two different frequencies (20 and 100 MHz) as shown in Fig. 3. As expected when a vertical dipole is used as Tx, the effect of the

Authorized licensed use limited to: Seoul National University. Downloaded on December 15,2022 at 13:59:12 UTC from IEEE Xplore. Restrictions apply.

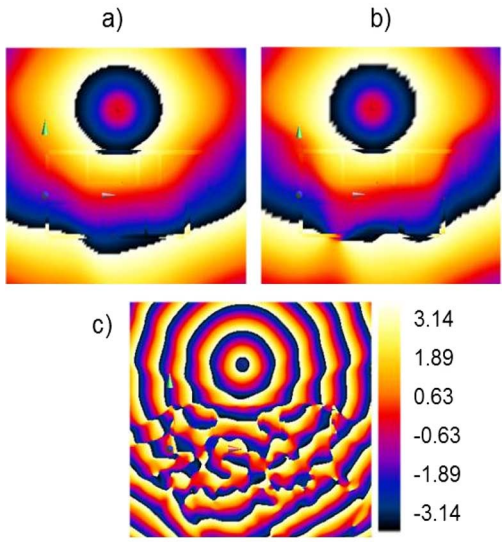

Fig. 4. Phase map of the geometry given in Fig. 2 where the Tx antenna is positioned at (9,10,1.5). The phase map is given in (a) with ground and dielectric walls and ceiling at 20 MHz, (b) with metallic scatterers in addition to dielectric scatterers at 20 MHz, and (c) with metallic scatterers in addition to dielectric scatterers at 100 MHz.

vertical metallic scatterers (used for reinforcing walls in realistic buildings) can be seen in the field coverage at both frequencies, but the horizontal metallic scatterers are not significant since the radiated field is vertically polarized. By comparing the field coverage plots in Fig. 3, we note that at 100 MHz the signal components scattered by the building walls, ground and ceiling become comparable to the direct field component causing significant fading and uneven field distribution. Of course, if the frequency is increased further (e.g., L or X band), the multipath level becomes even more significant [11], [12]. In addition, attenuation through the walls and ceilings becomes much larger making the possibility of source tracking using these frequencies challenging. We can see that the effect of the scatterers is much less prevalent at 20 MHz. The fact that the multipath level is very small and that the direct path is the dominant component of the total received field is the main reason the HF band is considered. In Fig. 4, the phase map for the geometry given in Fig. 2 are given. As can be seen, at 20 MHz (Fig. 4(a) and (b), even in the presence of dielectric and metallic scatterers, the phase fronts inside the building are only slightly disturbed. When the frequency is increased to 100 MHz (Fig. 4(c), the effect of the multipath becomes more significant. At a given frequency, the error introduced on the tracking resolution due to the small multipath is first calculated by performing simulations with and without the building walls. Then, the highest frequency at which the error is within the intended resolution of the system is selected. After the frequency of operation is chosen, the performance of the proposed tracking approach is investigated. Here, we discuss the results of three sets of simulations based on a FDTD full-wave solver. The building geometry considered is the same as that of Fig. 2. A detailed simulation setup and parameters are given in Fig. 5.

In the first simulation, only the dielectric scatterers were considered. This is important because many residential houses do not include metals and instead use bricks or wood. The goal here is to study the effect of having mostly dielectric scatterers on the

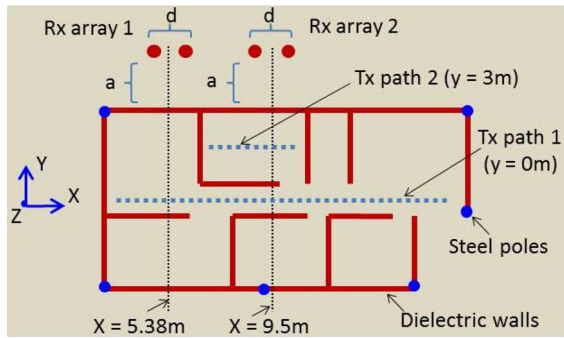

Fig. 5. Top view of the full-wave simulation setup. The geometry of the problem is the same as the one shown in Fig. 2. For this case, the Tx antenna is moved inside the building while the Rx array is positioned outside. The simulations in this section use z-directed short dipoles Tx and Rx antennas.

proposed source tracking technique. For this simulation, the receive array is kept stationary and the Tx antenna is moved along a straight line inside the building. For each Tx position, the received field at the receive antennas is recorded. It is obvious that when the Tx antenna is at the boresight of the Rx arrays ($x = 5.38$ m and $x = 9.5$ m for Rx array 1 and Rx array 2, respectively), the phase difference between the received signals is zero. In this case the Tx antenna is moved (along Tx path 1 in Fig. 5 to vary the phase differences between the received signals. The same analysis could have been done by fixing the position of the Tx antenna and rotating the Rx array to create the phase differences. The DOAs for a given position of the Tx antenna are calculated from the center of both receive arrays. These DOA values are then used to compute the location of the Tx antenna based on the technique describe in Section II. The plots given in Fig. 6 show the DOA calculated based on the phase and magnitude of the signals received by the two Rx antennas of array 1. For comparison, the same setup (without the walls) is simulated based an asymptotic Dyadic Green's function for a half-space medium which takes into account the near-ground propagation effects [19]. As described in the original work, by utilizing asymptotic Dyadic Green's function, the Norton surface waves that become prevalent in near-ground scenarios can be fully taken into account. The results confirm that even in the presence of scatterers such as walls and ground, the DOA of the signal can be successfully retrieved because the direct signal is dominant compared to the level of multipath in the HF band. It should be noted that the errors in the estimated DOA are caused by small level of multipath that still exists (it is much smaller than the direct path) and antenna coupling in the Rx array especially for larger DOA values which is described in Section III.B. It should be noted that the proposed system needs to measure only small DOAs because the Rx arrays which are positioned on a rotating platform can rotate to keep the Tx antenna along the bisect of the Rx array. Essentially, as the Tx antenna moves, the Rx array rotates in such a way that the phase difference between the received signals at the Rx elements is at a global minima. The advantage of this approach is that the system does not have to measure large DOA values and hence can avoid DOA errors that can be significant [see Fig. 6(a)].

A second set of simulations for a more complex scenario is also performed. Since some buildings are built out of both

Authorized licensed use limited to: Seoul National University. Downloaded on December 15,2022 at 13:59:12 UTC from IEEE Xplore. Restrictions apply.

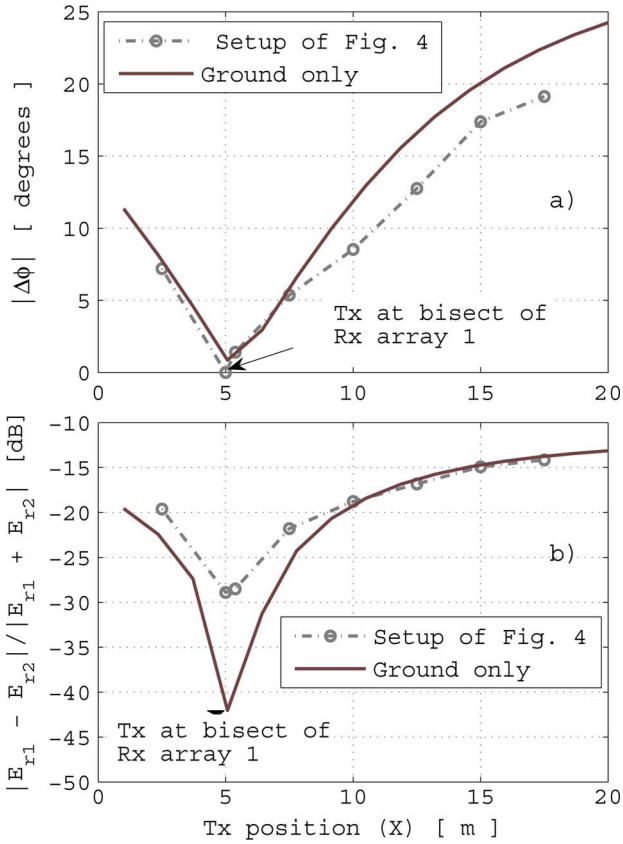

Fig. 6. Geometry of the simulation is given in Fig. 4 ($d = 1.25\ m, a = 1\ m$). The source is moved along Tx path 1 and phase difference variation of the received signals at Rx array 1 is plotted in (a) and the magnitude of the received signals are used to calculate DOA based (2) (b).

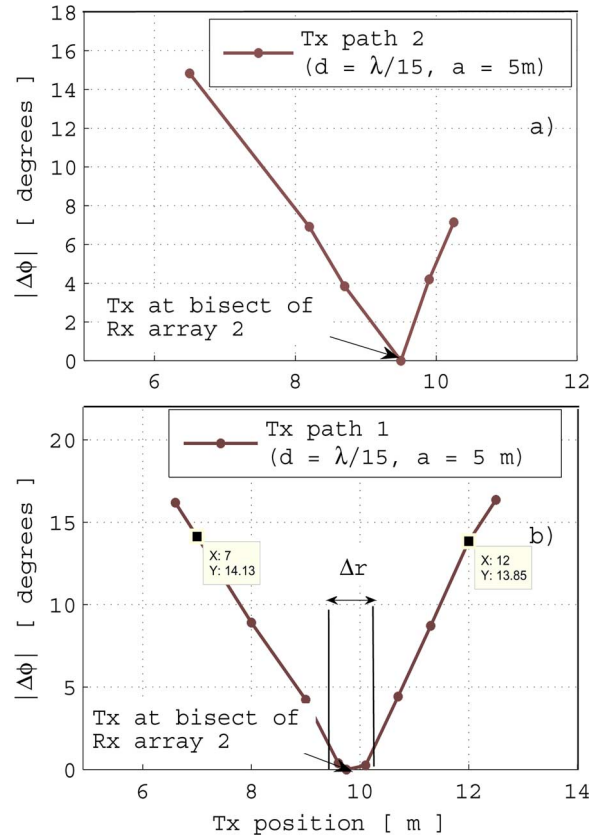

Fig. 7. Geometry of the simulation is given in Fig. 5 ($d = 1\,\mathrm{m}, a = 5\,\mathrm{m}$). Phase difference variation of the received signals at Rx array 2 when the source moves along Tx path 1 (b) and Tx path 2 (a) are shown. Dielectric walls and metallic scatterers for the walls and ceiling are included in this simulation (Fig. 2).

metallic and dielectric materials, the performance of the proposed direction finding technique must be analyzed in the presence of both types of scatterers. For this simulation, thick cylindrical posts are placed at the various corners and junctions of the building (Fig. 2. A pair of short dipoles are used as a receive array (the bisect of the array is along $x = 9.5$). The received fields at each antenna is recorded by running the FDTD solver for various positions of the Tx antenna (Tx path 1 and Tx path 2 shown in Fig. 5. As can be seen in Fig. 7(a), when the Tx antenna is moved along Tx path 2, the phase difference plot results in a null at the bisect of Rx array 2. Tx path 1 is also considered to investigate the performance of the proposed technique for various locations inside the building. Fig. 7(b), the result for the case where the source moves along Tx path 1, shows a null at the correct location. Of course, there is a relatively small error in the estimated DOA values. For example, in Fig. 7(b), we notice that when the Tx antenna is at $\mathrm{x} = 7$ (2.5 m to the left of the bisect of Rx array 2, see Fig. 4), the estimated phase difference is 14.13°. On the other hand, when the Tx antenna is at $\mathrm{x} = 12$ (2.5 m to the right of the bisect of Rx array 2), the estimated phase difference is 13.85°. The calculated phase difference based on the location of the Tx and Rx antennas is 14.03° for both cases. So, the errors in the retrieved phase differences are small (despite the presence of indoor scatterers). For this simulation d is 1 m and a is 5 m.

In the third simulation, the effect of increased multipath level is investigated by comparing phase differences at 20 MHz and 40 MHz with the same geometry as the above two cases. The

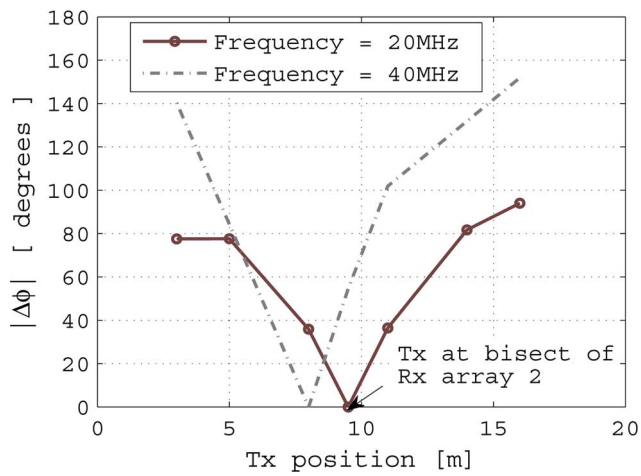

Fig. 8. Geometry of the simulation is given in Fig. 4 ($d = 1.25\,\mathrm{m}, a = 1\,\mathrm{m}$). Phase difference variation of the received signals at Rx array 2 is plotted at 20 MHz and 40 MHz (for Tx path 1). Dielectric walls and metallic scatterers are included.

phase differences between the received signals at Rx array 2 are computed as the Tx antenna is moved along Tx path 1. The plots in Fig. 8 show that the error in estimated phase differences increase as the frequency is increased because the effect of the scatterers becomes more significant at 40 MHz compared to 20 MHz. To investigate the effect nearby scatterers, the receive array for this case was positioned very close to the wall unlike the previous case ($a = 1$ m). The bisect of the receive array is

Authorized licensed use limited to: Seoul National University. Downloaded on December 15,2022 at 13:59:12 UTC from IEEE Xplore. Restrictions apply.

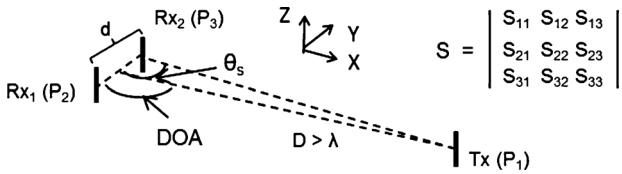

Fig. 9. Three antenna system used for antenna coupling analysis.

TABLE II
ANTENNA COUPLING ANALYSIS USING FULL-WAVE SIMULATION (SEE FIG. 9)

d [λ]	DOA [°]	$\lvert DOA_{est} - DOA_{exact}\rvert$[°]
$\lambda/15$	53.1	1.5
$\lambda/15$	64.6	0.9
$\lambda/15$	80	0.3
$\lambda/15$	90	0
$\lambda/15$	100	0.3

correctly retrieved only at 20 MHz. The slight asymmetry compared to the previous case (Fig. 7 in the result is caused by the close proximity of the antennas to the wall.

B. Antenna Coupling Analysis

Because of the close proximity of the antenna elements in the receive array $(\lambda/15)$, the effect of the interelement coupling has to be investigated. One way to analyze the coupling as it relates to direction finding is by using the scattering matrix (S-matrix) of the antenna system. The three antenna system consisting of the Tx antenna and the two Rx antennas on the receive array can be modeled as a three port network which can be represented by a 3×3 S-matrix (Fig. 9. Because of Lorentz reciprocity, the S-matrix is symmetric. For our application, S_{12} and S_{13} are the important elements since these elements are responsible for interelement coupling between the receive antennas. S_{12} can be calculated by first exciting the Tx antenna (port P_1) and measuring the voltage at port P_2 while P_3 is matched to 50 Ω. S_{12} is then computed by taking the ratio of V_1 to V_2. When the two Rx antennas are illuminated by the radiated field from the Tx antenna, the scattering from Rx_2 induces a voltage across the port of Rx_1 and vice versa. So, the received field at Rx_1 consists of the direct field from the Tx antenna and a small scattered component from Rx_2 determined by the radar cross-section of the short dipole and the scattering angle (θ_s). To quantify the effect of antenna coupling on the retrieved DOA, a full-wave simulation consisting of three short dipoles is carried out with no other scatterers present (Fig. 9). The error in the retrieved DOA is then calculated by taking the difference between the retrieved DOA (from simulation) and exact DOA (based on geometry). It should be noted that when the Tx antenna is at the bisect of the two identical receive antennas, the error in phase difference due to antenna coupling is zero. If the Tx moves on the azimuth plane (the x-y plane in Fig. 9, a small error is introduced on the phase difference. The results of the full-wave simulation (errors due antenna coupling) are shown in Table II. The results show, for small antennas whose bistatic scattering is almost invariant with the bistatic angle, the resulting errors are quite small. The coupling effect has been fully taken into account in the full-wave simulation analysis presented in Section III.B. Also, a scenario where the dipole lengths are slightly different was simulated. There was no significant change in the error compared to identical antennas.

IV. SOURCE TRACKING SYSTEM PROTOTYPE

Having performed numerical analysis of direction finding in multipath environments, the next step is to validate our proposed approach using measurement results. In order to realize the proposed system, various components need to be designed, fabricated and tested. Assuming a narrowband signal in the HF range is transmitted by the miniaturized antenna, the signals at the two receiving antennas are first filtered by narrowband, low-loss filters with high stop-band rejection. The filtering stage is important to reduce the out-of-band noise and maximize SNR as much as possible. Assuming a zero-mean Gaussian noise, the standard deviation of phase in terms of SNR is given by $\sigma_\phi = 57.3^\circ/\sqrt{\mathrm{SNR}}$. The SNR is an important quantity because it is the main limiting factor determining the smallest phase difference that can be accurately measured which in turn affects the maximum tracking resolution. After the filtering stage, the signals are amplified by low-noise, high-gain amplifiers. Since the components used could introduce phase differences between the two signal lines, an electronic phase shifter is connected in one of the lines for calibration. The next component which is the PDA circuit (discussed in Section IV.B) is a four-port passive network inspired by the hearing mechanism of a fly that essentially amplifies the phase difference between the input signals into a much larger value that can then be measured accurately. The output signals of the phase difference amplification (PDA) circuit are sampled by a highly sensitive two channel 16-bit A/D converter. In this section, we will first describe the design and fabrication of a miniaturized low-profile HF antenna. The principles of operation and design of the four-port PDA circuit is also described. We concluded the section with test results performed in various environments.

A. Highly Miniaturized Low-Profile HF Antenna

Conventional antennas in the HF range are prohibitively large especially for applications such as tracking of small robotic platforms where the antennas are to be integrated. For our prototype, a very low-profile miniaturized antenna with vertical polarization and omnidirectional pattern, operating in the HF band is utilized. The length and width of the antenna are both $\lambda/100$ while the height is $\lambda/300$ at 20 MHz. For such extremely low-profile condition, the radiation efficiency becomes very small. One way of improving the gain of low-profile vertically polarized antenna is to use multiple vertical elements in phase which is equivalent to having a vertical short dipole with higher height. This approach is used to design the Tx antenna in the proposed source tracking system. In order to minimize the size of the vertically polarized antenna with two in-phase vertical elements, a modified T-type 180° phase shifter utilizing a capacitive impedance inverter is used [22]. As can be seen in Fig. 10(a), the currents on the feed and shorting pins (I_1 and I_2) that would normally have 180° phase difference are forced to flow in the same direction by using a T-type 180° phase shifter. First, the capacitance value is determined by the limited area of the capacitive plate (150 mm $\times$ 150 mm). Next, in order to achieve 180° phase shift of the T-type phase shifter at the frequency of interest, the inductance value is calculated. The values used in our design are $\mathrm{L} = 10\ \mu\mathrm{H}$ and $\mathrm{C} = 10$ pF. It should be noted that these values

Authorized licensed use limited to: Seoul National University. Downloaded on December 15,2022 at 13:59:12 UTC from IEEE Xplore. Restrictions apply.

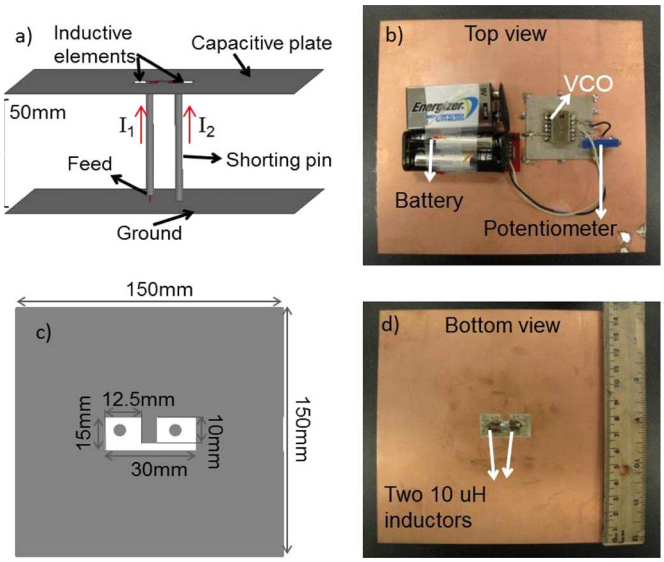

Fig. 10. Low profile miniaturized antenna designed to operate at 22.8 MHz and the optimized dimensions are shown (a), (c). The top and bottom view of the fabricated antenna are shown in (b) and (d), respectively. The inductive and capacitive elements form a realization of a 180° T-type phase shifter. This forces I_1 and I_2 to be in phase (a).

are just for ideal circuit simulations. In the actual antenna geometry, the parasitic inductance of feeding and shorting pins and dielectric constant of thin substrates of top and bottom plates also affects the values. For this antenna, a lumped element capacitor can not be used as that would cause an out-of-phase conduction current to the ground which would result in radiation cancellation. For this reason, the required capacitor is realized by using an open stub. Finally, for a given lateral dimension and height, the miniaturized antenna structure is designed by optimizing the geometry of the open stub to get omnidirectional radiation pattern. The proposed antenna was successfully fabricated and integrated with voltage controlled oscillator (VCO) operating at HF-band and a battery, as shown in Fig. 10. The VCO is used to tune the frequency of operation. Having the battery integrated with the antenna is important because if a cable is used to feed the antenna, the cable itself will become part of the antenna (λ at 23 MHz is $\sim$ 13 m), leading to a shift in the resonant frequency, poor impedance matching and radiation pattern. The measured antenna gain is -29.2 dBi, which is similar to the simulated gain of -28.1 dBi. In comparison, the gain of the spiral-shaped inverted-F antenna (IFA) is -34.4 dBi which is 5.2 dB lower than that of the proposed antenna. The radiation pattern of the proposed antenna is given in Fig. 11.

B. Phase Difference Amplification (PDA) Circuit Inspired by Ormia's Hearing Mechanism

The receive end in our system prototype consists of two antennas operating in the HF range that are very close to each other in terms of wavelength ($\lambda/15$ at 20 MHz). One of the challenges that arise at such low frequencies is that the phase difference between the two received signals becomes too small to be accurately measured. Also, the resolution of tracking is limited by the smallest phase difference that can be measured. The smallest measurable phase difference is in turn determined

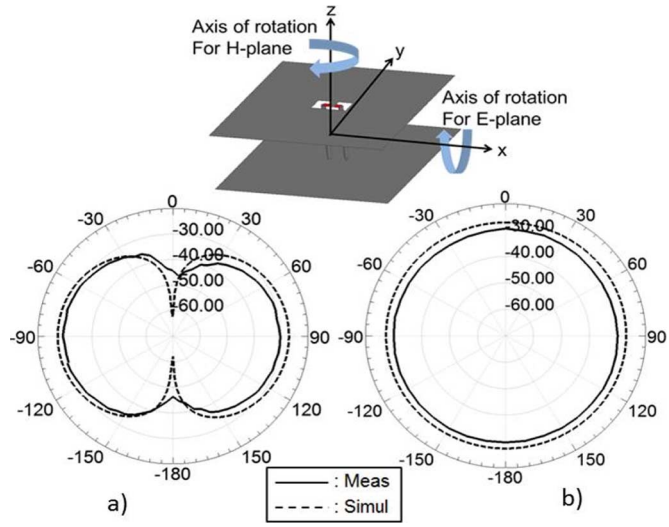

Fig. 11. Measured and simulated radiation patterns of the proposed antenna in (a) E($=$ yz) plane and (b) H($=$ xy) plane.

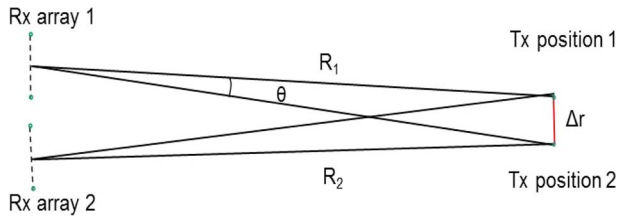

Fig. 12. Geometry used to analyze the minimum phase requirement for a given tracking resolution.R_1 and R_2 are the distances between the center of the Rx arrays to the first and second positions of the source.

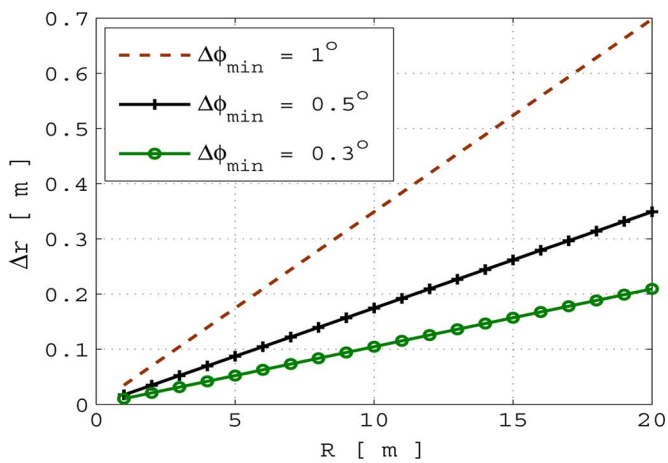

Fig. 13. Azimuth resolution plotted against Tx-Rx separation. The three curves show the resolution for various values of minimum phase difference between received signals that can accurately be measured ($\Delta\phi_{\min}$).

by the SNR. Given a receive array and a Tx antenna as depicted in Fig. 12, the phase difference between the signals at the Rx antennas changes slightly as the Tx antenna moves a distance Δr. If the system can accurately measure the phase difference introduced because of the motion of the Tx antenna, then that means the system can achieve a spatial resolution of Δr. A plot that relates the spatial resolution to Tx-Rx separation and the minimum phase difference that can be measured is presented in Fig. 13. For example, if the system can accurately measure a phase difference of 1° and the Rx antennas on the array is separated by 1 m, then the best possible spatial tracking resolution

Authorized licensed use limited to: Seoul National University. Downloaded on December 15,2022 at 13:59:12 UTC from IEEE Xplore. Restrictions apply.

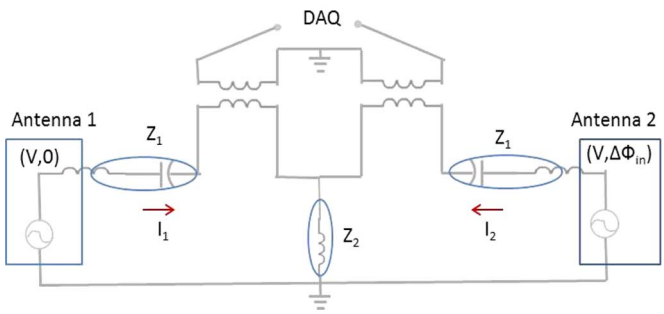

Fig. 14. Phase difference amplification circuit designed to amplify small phase differences.

is about 35 cm for a Tx-Rx separation of 10 m. Since the measurement of small phase differences is challenging, we need a way to enhance the accuracy in phase difference measurement without increasing the baseline distance.

To tackle the challenge associated with measuring very small phases, we utilize a phase difference amplification technique inspired by the hearing mechanism of a fly called Ormia Ochracea. Ormia is a small fly which is known for its accurate directional hearing. This ability helps Ormia loacalize the mating call of the male cricket. Ormia's ears are separated by a mere 1.2 mm ($\lambda/60$ at 4.5 KHz). This close proximity causes the arrival times of the sound pressures at the two ears to be less than 1 to 2 μs [23], [24]. So, how is that Ormia can sense the direction of sound with resolution as small as 1°? Ormia uses a sophisticated structure that mechanically couples its two ears, the effect of which is the amplification of the phase difference to values that are amenable to neural processing. The electrical analogous of Ormia's phase difference amplification mechanism is first investigated in [25]. The schematic in Fig. 14 shows a realization of this approach. The coupling circuit consists of various lumped elements and two transformers used to measure currents I_1 and I_2. So, by optimizing the values of the lumped elements, the phase difference between I_1 and I_2 dramatically increases compared to the phase differences between the input signals. Assuming the amplitudes of the input signals are almost the same, the output phase difference ($\Delta\phi_{\text{out}} = |\phi(I_2) - \phi(I_1)|$) can be approximated in terms of the input phase difference (phase difference between the received fields at the two Rx antennas) as

$$\Delta\phi_{\text{out}} = \angle\left(\frac{e^{j\Delta\phi_{\text{in}}} - K}{1 - e^{j\Delta\phi_{\text{in}}}}\right), \qquad K = \frac{Z_2}{Z_2 + Z_1} \tag{3}$$

where $\Delta\phi_{\text{out}}$ the output phase difference. Z_1 and Z_2 are the series and shunt impedances, respectively (as given in Fig. 14). To get an insight into how the circuit works, let us look at two extreme cases which are when the impedance of Z_2 is zero and infinity. When $Z_2 = 0$ ($K = 0$), the output phase difference will be same as the input phase difference. On the other hand, if Z_2 is very large ($K \sim 1$), the phase difference becomes $\sim 180°$. When Z_2 is finite and larger than Z_1, the phase difference between the two currents will be an amplified version of the original phase difference. The way this circuit is optimized is based on the following two conditions: 1) Achieving the desired phase amplification which is determined by the phase amplification factor (K); and 2) Maximizing the power at the output channels of the PDA circuit (by achieving impedance matching at each stage of the receive circuit). The values chosen in the final design are $K = 0.84$ and $Z_1 = j120\ \Omega$. The circuit was fabricated and tested using a signal generator, an electronic phase shifter and an A/D converter. As can be seen in Fig. 15, there is a very good agreement between measured and simulated results. It should be noted that this circuit is only necessary when the input phase differences are relatively small ($\leq 10°$). Larger input phase differences can be directly measured without amplification.

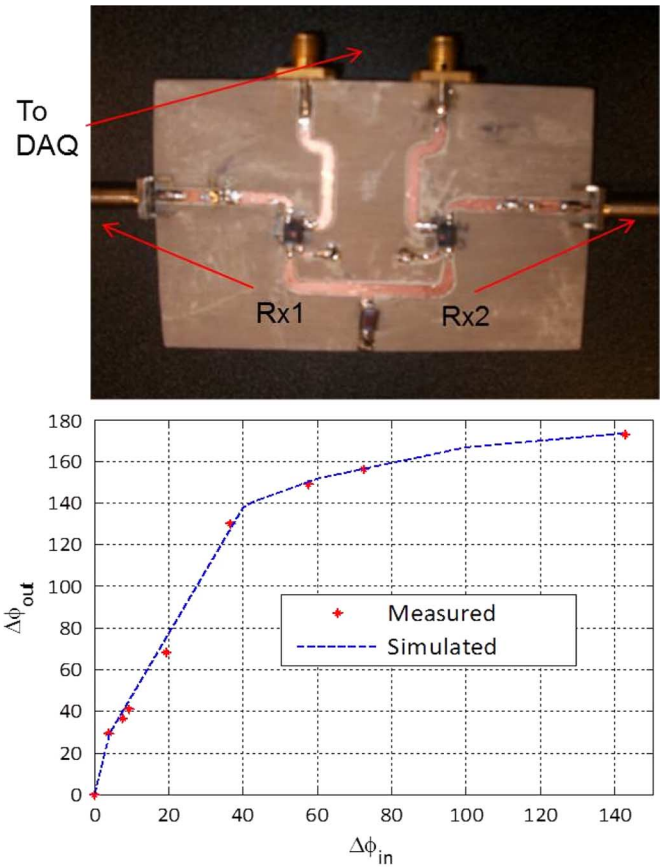

Fig. 15. Picture of the fabricated PDA circuit where Rx1 and Rx2 are the ports that connect to the two receive antennas is shown. The simulation and measurement results of the phase difference amplification are given in the plot.

C. System Integration and Test

The receiver module as can be seen in Fig. 16 consists of two signal lines each having a narrowband, low-loss filter connected to the two miniaturized dipole antennas ($\sim \lambda/15$). A high-gain low-noise amplifier is then used to amplify each signal by about 40 dB. However, the noise that passes through the filters with the signal of interest will also be amplified. It's vital to minimize this noise to achieve the maximum possible SNR. For this reason, a second set of band-pass filters with high stop-band rejection are used. The various parameters of the system are listed in Table III. The second column in the table lists the calculated or simulated values for the Tx antenna gain (G_t), Rx antenna gain (G_r), the output power of the VCO used to feed the Tx antenna (P_{Source}), the received power (P_r) and the distance between the Tx and Rx antennas (R). The third column of the

Authorized licensed use limited to: Seoul National University. Downloaded on December 15,2022 at 13:59:12 UTC from IEEE Xplore. Restrictions apply.

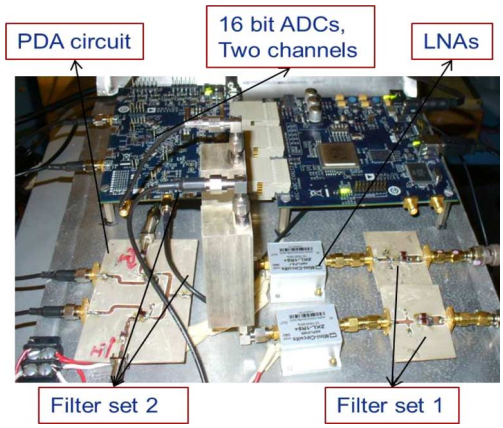

Fig. 16. Receiver module including a sensitive pair 16 bit ADCs, phase amplification circuit, various filters, amplifiers.

TABLE III
COMPARISON OF CALCULATED AND MEASURED RECEIVED SYSTEM PARAMETERS

	Calculated/Simulated	Measured
Gt [dB]	−26	−28
Gr [dB]	−12	−13
Freq. [MHz]	22.8	22.8
$\lambda[m]$	13.27	13.27
$P_{Source}[dBm]$	8	8
$P_r[dBm]$	−55.54	−53
$R[m]$	20	20

table lists measured values for the same parameters. The antenna gains were measured outside where the multipath effects were minimized by positioning one antenna at higher elevation relative to the other antenna [22].

With the current setup, at the maximum Tx-Rx separation considered (20 m), an SNR well over 27 dB was achieved. It should be noted that this noise is not thermal noise, but is caused by signal interference and thus the error generated by it in both channels are coherent. This makes it possible to improve the DOA measurement by subtracting the coherent components and hence thermal noise uncertainty is not the main factor. Also, one way to improve the current system is by designing extremely narrowband filters with high stop-band rejection which will further improve the signal-to-interference ratio (SIR). The downside to using filters in the HF band based on lumped element components is that such filters suffer from low Q and/or high insertion loss. Other types of filters such as dielectric resonator filters and coaxial resonator filters which usually have high Q maybe used for better accuracy.

The Tx and Rx antennas are also tuned to maximize transmit and receive power, respectively. Without any amplifiers and filters, the received power is −53 dBm at 20 m Tx-Rx separation. As can be seen in Table III, the received power is similar to the expected value. This measurement was done both indoor and outside using a spectrum analyzer to estimate the SIR. The fact that we get similar received power results for both the indoor and outdoor cases further confirms the minimal effect of multipath at this frequency. For a Tx–Rx separation of varying from 5 to 20 m, the source tracking system was tested in various environments. We first tested the system for cases where there was

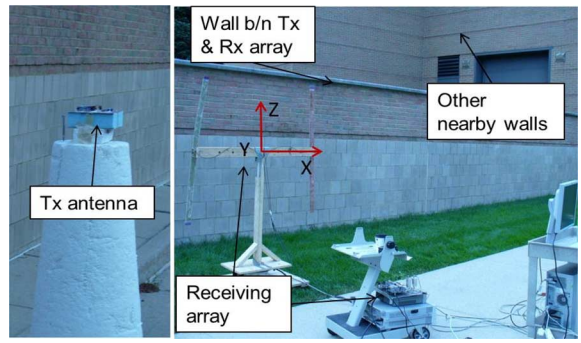

Fig. 17. Measurement setup of Case 3 in Table III (NLOS case), Tx was positioned at the boresite of the receiving array on the x-y plane. The Rx array and is then rotated about the z-axis to investigate the phase difference variation.

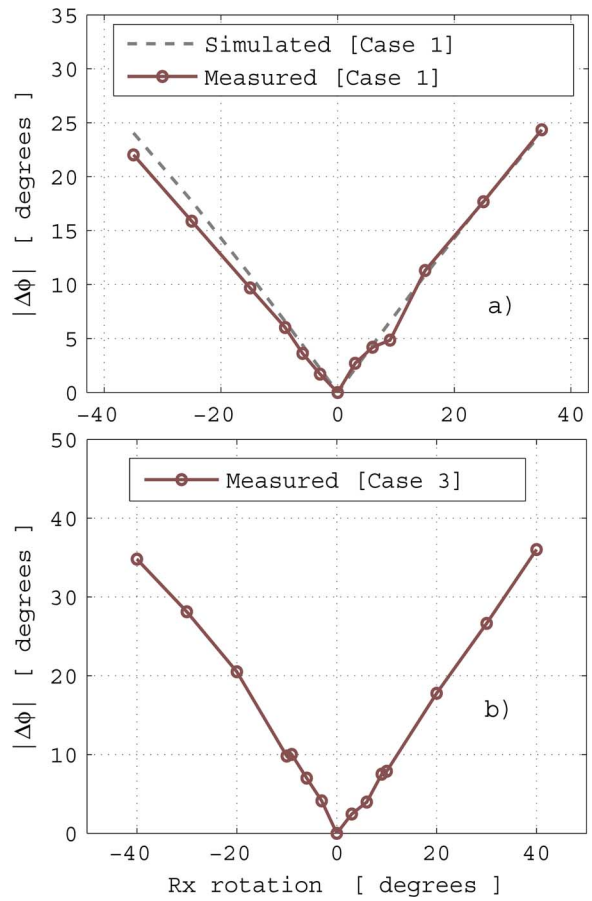

Fig. 18. Measurement results and comparison with simulation for the cases listed in Table IV.

a line of sight between the Tx and Rx antennas. The measured results were also compared with simulated results based on the half-space dyadic Green's function to capture the effect of the ground accurately. In all the measurements presented, the signals at the Rx antenna elements are recorded by keeping the Tx antenna stationary and rotating the Rx array in the azimuth plane about the center of the Rx array (one case is shown in Fig. 17). In the results that follow, we choose 0° rotation as the case when the Tx antenna is at the bisect of the Rx array. In Fig. 18(a), the phase difference comparison between measured and simulated results for Case 1 (see Table IV) show very good agreement. The mean error for this case is 0.78°. For each Tx position, the phase

Authorized licensed use limited to: Seoul National University. Downloaded on December 15,2022 at 13:59:12 UTC from IEEE Xplore. Restrictions apply.

TABLE IV
SOURCE TRACKING SYSTEM TEST SCENARIOS

Case	Tx/Rxs location	Line of sight?	Main Scatterers
1	Outdoor/Outdoor	Yes	Ground
2	Indoor/Indoor	Yes	Ground & Walls
3	Indoor/Indoor	No	Ground & Walls

TABLE V
COMPARISON OF THE PROPOSED SYSTEM WITH EXISTING TECHNIQUES [26], [27]

System	DOA accuracy [°]	Meas. scenario
TCI7235 (Wattson-Watt)	10	Free space
DDF255 (Rohde & Schwarz)	2	Free space
TCI 802C (Wattson-Watt)	2	Free space
Proposed system	≤ 1	Indoor,outdoor

difference is measured a minimum of five times. Errors are then calculated based on measurement and simulated results.

More importantly, the two channel 80MSPS A/D converter acquires about 16 000 samples. The FFT process essentially averages over the samples in 0.2 ms (averages over 4000 cycles of the signal). The FFT process along with the use of very narrowband filters reduces the noise power which in turn decreases the effective receiver bandwidth. The thermal noise power is calculated using $N = KTB$, where K, T and B are Boltzmann's constant, the temperature and the effective receiver bandwidth, respectively (N is the noise power). The uncertainty in phase measurement can then be calculated based on the resulting SNR using $\sigma_\phi = 57.3°/\sqrt{\mathrm{SNR}}$ as alluded to earlier. For our system, the uncertainty in phase measurement is well within 1°. By referring to Fig. 13, we see that the error in the retrieved DOA results in a spatial tracking resolution of about 70 cm. The slight asymmetry in the measured result and the overall error is caused by measurement errors and the effect of antenna coupling between the Rx antennas as discussed in Section III.C. Measurement errors come from inaccuracy in determining the location of the antennas especially for NLoS scenarios and differences in the performance of Rx antenna elements. The small multipath effect also contributes to the error. The result in Fig. 18(b) (Case 3, Table IV) shows that the proposed system works in NLOS case as well. The setup for this case is given in Fig. 17.

It is worth comparing the proposed system to the state of the art commercial DF systems. In the literature there are not many HF DOA retrieval techniques and measurement results for NLoS environments that we could make direct comparison with. Table V lists a few commercial systems and their accuracy compared to the proposed system.

V. CONCLUSION

A Sub-wavelength RF source tracking technique utilizing highly miniaturized HF antenna for applications in GPS-denied environments such as indoor and urban scenarios is proposed. Numerical models are used to investigate wave propagation and scattering in complex indoor scenarios as a function of frequency and analyze the possibility of direction finding in the HF range in the presence dielectric and metallic scatterers. The proposed approach is based on a radio triangulation approach in conjunction with a direction retrieval approach utilizing a highly miniaturized Tx antenna and a compact Rx antenna array. A system prototype has also been implemented and tested. A low-profile and highly miniaturized antenna ($\lambda/300$ height and $\lambda/100$ lateral dimensions at 20 MHz) designed to efficiently generate omnidirectional vertically polarized field is designed and fabricated. At such low frequencies, since the phase difference between the signals at the Rx antenna pairs is too small to be accurately measured, a biomimetic circuit that mimics the hearing mechanism of a fly (Ormia Ochracea) is utilized. With this circuit, very small phase differences are amplified to values that can easily be measured. The system prototype has been tested for various scenarios with different levels of multipath. The test results show that a source in a complex GPS-denied environment can be successfully localized using the proposed approach.

REFERENCES

[1] T. Li, A. Ekpenyong, and Y.-F. Huang, "Source localization and tracking using distributed asynchronous sensor," *IEEE Trans. Signal Process.*, vol. 54, no. 10, pp. 3991–4003, Oct. 2006.

[2] [Online]. Available: http://www.crfs.com/technology/direction-finding/

[3] Z. Wang and S. A. Zekavat, "Manet localization via multi-node TOA-DOA optimal fusion," in *Proc. IEEE Military Commun. Conf.*, 2006, pp. 1–7.

[4] B. N. Hood and P. Barooah, "Estimating DoA from radio-frequency RSSI measurements using an actuated reflector," *IEEE Sens. J.*, vol. 11, no. 2, pp. 413–417, Feb. 2011.

[5] A. H. El Zooghby, C. G. Christodoulou, and M. Georgiopoulos, "A neural network-based smart antenna for multiple source tracking," *IEEE Trans. Antennas Propag.*, vol. 48, no. 5, pp. 768–776, Nov. 2000.

[6] Y. Wang, G. Leus, and H. Delic, "TOA estimation using uwb with low sampling rate and clock drift calibration," in *Proc. IEEE Int. Conf. Ultra-Wideband*, 2009, pp. 612–617.

[7] P. Z. Alba, V. Josep, and D. H. Brooks, "Closed-form solution for positioning based on angle of arrival measurements," in *Proc. 13th IEEE Int. Symp. Personal Indoor Mobile Radio Comm.*, 2002, vol. 4, pp. 1522–1526.

[8] F. Belloni, V. Ranki, A. Kainulainen, and A. Richter, "Angle-based indoor positioning system for open indoor environments," in *Proc. 6th Workshop Position., Nav., Commun.*, 2009.

[9] L. Cong and W. H. Zhuang, "Hybrid TDOA/AOA mobile users location for wideband CDMA cellular systems," *IEEE Trans. Wireless Commun.*, vol. 1, pp. 439–447, Jul. 2002.

[10] C.-D. Wann, Y.-J. Yeh, and C.-S. Hsueh, "Hybrid TDOA/AOA indoor positioning and tracking using extended Kalman filters," in *Proc. IEEE Conf. Veh. Technol.*, Sep. 2006, pp. 1058–1062.

[11] W. T. Barnett, "Multipath propagation at 4,6, and 11 GHz," *Bell Syst. Tech. J.*, vol. 51, no. 2, pp. 321–361, Feb. 1972.

[12] C. L. Ruthroff, "Multiple-path fading on line-of-sight microwave radio systems as a function of path length and frequency," *Bell Syst. Tech. J.*, vol. 50, no. 7, pp. 2375–2398, Sep. 1971.

[13] C. Morelli, M. Nicoli, V. Rampa, and U. Spagnolini, "Hidden markov models for radio localization in mixed LOS/NLOS condition," *IEEE Trans. Signal Process.*, vol. 55, no. 4, pp. 1525–1542, Apr. 2007.

[14] C. K. Seow and S. Y. Tan, "Non-line-of-sight localization in multipath environments," *IEEE Trans. Mobile Comput.*, vol. 7, no. 5, pp. 647–660, May 2008.

[15] D. E. Gustafson, M. S. Bottkol, J. R. Parry, J. M. Elwell, and T. Q. Nguye, "Indoor geolocation using RF multipath with probabilistic data association," in *Proc. IEEE Locat. Nav. Symp.*, May 2008, pp. 402–412.

[16] S. L. Cotton, W. G. Scanlon, and B. K. Madahar, "Millimeter-wave soldier-to-soldier communications for covert battlefield operation," *IEEE Commun. Mag.*, vol. 47, no. 10, pp. 72–81, Oct. 2009.

[17] M. K. Kaise, N. R. Gans, and W. E. Dixon, "Vision-based estimation for guidance, navigation, and control of an aerial vehicle," *IEEE Trans. Aerosp. Electron. Syst.*, vol. 46, no. 3, pp. 1064–1077, Jul. 2010.

[18] W.-H. Liau, C.-L. Wu, and L.-C. Fu, "Inhabitants tracking system in a cluttered home environment via floor load sensor," *IEEE Trans. Autom. Sci. Eng.*, vol. 5, no. 1, pp. 10–20, Jan. 2008.

Authorized licensed use limited to: Seoul National University. Downloaded on December 15,2022 at 13:59:12 UTC from IEEE Xplore. Restrictions apply.

[19] D. Liao and K. Sarabandi, "Near-earth wave propagation characteristics of electric dipole in presence of vegetation or snow layer," *IEEE Trans. Antennas Propag.*, vol. 53, no. 11, pp. 3747–3756, Nov. 2005.
[20] F. T. Dagefu and K. Sarabandi, "Analysis and modeling of near-ground wave propagation in the presence of building walls," *IEEE Trans. Antennas Propag.*, vol. 59, no. 6, pp. 2368–2378, Jun. 2011.
[21] M. Thiel and K. Sarabandi, "3D-wave propagation analysis of indoor wireless channels utilizing hybrid method," *IEEE Trans. Antennas Propag.*, vol. 57, no. 5, pp. 1539–1546, May 2009.
[22] J. Oh, J. Choi, F. T. Dagefu, and K. Sarabandi, "Extremely small multi-element monopole antenna with enhanced gain," *IEEE Trans. Antennas Propag.*, submitted for publication.
[23] M. Akcakaya and A. Nehorai, "Performance analysis of the Ormia Ochracea's coupled ears," *J. Acoust. Soc. Amer.*, vol. 124, no. 4, pp. 2100–2105, Oct. 2008.
[24] R. N. Miles, D. Robert, and R. R. Hoy, "Mechanically coupled ears for directional hearing in the parasitoid fly Ormia Ochracea," *J Acoust. Soc Amer.*, vol. 98, no. 6, pp. 3059–3070, Dec. 1995.
[25] N. Behdad, M. A. Al-Joumayly, and M. Li, "Biologically inspired electrically small antenna arrays with enhanced directional sensitivity," *IEEE Antennas Wireless Propag. Lett.*, vol. 10, pp. 361–364, Apr. 2011.
[26] [Online]. Available: http://www.sorrac.com
[27] [Online]. Available: http://www.rohde-schwarz.us

Fikadu T. Dagefu (S'07) received the B.S. degree in electrical engineering from the University of Texas at Austin in 2007 and the M.S. degree in electrical engineering from the University of Michigan, Ann Arbor in 2009 where he is currently pursuing his Ph.D. degree also in electrical engineering (Applied Electromagnetics). His research interests include radar remote sensing, source tracking in complex GPS-denied environments and wave propagation modeling/measurements.

Mr. Dagefu is the recipient of the 2011 MIT Lincoln Laboratory Graduate Fellowship. He was also a finalist in the student paper competitions at the IEEE IGARSS international conference in 2009 and 2010.

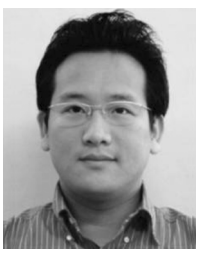

Jungsuek Oh (S'08) received the B.S. and M.S. degrees from Seoul National University, Korea, in 2002 and 2007, respectively, and the Ph.D. degree from the University of Michigan at Ann Arbor, in 2012. From 2002 to 2005, he worked as an associate software engineer in Kong Young DBM, Korea. From 2007 to 2008, he was with Korea Telecom as an associate research engineer working on the development of flexible RF devices.

He is currently a Research Fellow with the Radiation Laboratory, the University of Michigan. His research areas include antenna miniaturization for integrated systems and radio propagation modeling for indoor scenarios. He is the recipient of the 2011 Rackham Predoctoral Fellowship Award at the University of Michigan.

Kamal Sarabandi (S'87–M'90–SM'92–F'00) received the B.S. degree in electrical engineering from the Sharif University of Technology, Tehran, Iran, in 1980, the M.S. degree in electrical engineering in 1986, and the M.S. degree in mathematics and the Ph.D. degree in electrical engineering from The University of Michigan at Ann Arbor in 1989.

He is currently the Director of the Radiation Laboratory and the Rufus S. Teesdale Professor of Engineering in the Department of Electrical Engineering and Computer Science, The University of Michigan at Ann Arbor. His research areas of interest include microwave and millimeter-wave radar remote sensing, meta-materials, electromagnetic wave propagation, and antenna miniaturization. He possesses 25 years of experience with wave propagation in random media, communication channel modeling, microwave sensors, and radar systems and leads a large research group including two research scientists, 16 Ph.D. students. He has graduated 40 Ph.D. and supervised numerous post-doctoral students. He has served as the Principal Investigator on many projects sponsored by the National Aeronautics and Space Administration (NASA), Jet Propulsion Laboratory (JPL), Army Research Office (ARO), Office of Naval Research (ONR), Army Research Laboratory (ARL), National Science Foundation (NSF), Defense Advanced Research Projects Agency (DARPA), and a large number of industries. Currently he is leading the Center for Microelectronics and Sensors funded by the Army Research Laboratory under the Micro-Autonomous Systems and Technology (MAST) Collaborative Technology Alliance (CTA) program.

He has published many book chapters and more than 220 papers in refereed journals on miniaturized and on-chip antennas, meta-materials, electromagnetic scattering, wireless channel modeling, random media modeling, microwave measurement techniques, radar calibration, inverse scattering problems, and microwave sensors. He has also had more than 500 papers and invited presentations in many national and international conferences and symposia on similar subjects.

Dr. Sarabandi served as a member of NASA Advisory Council appointed by the NASA Administrator for two consecutive terms from 2006–2010. He is serving as a vice president of the IEEE Geoscience and Remote Sensing Society (GRSS) and is a member of the Editorial Board of the PROCEEDINGS OF THE IEEE. He was an associate editor of the IEEE TRANSACTIONS ON ANTENNAS AND PROPAGATION and the IEEE SENSORS JOURNAL. He is a member of Commissions F and D of URSI. Dr. Sarabandi was the recipient of the Henry Russel Award from the Regent of The University of Michigan. In 1999 he received a GAAC Distinguished Lecturer Award from the German Federal Ministry for Education, Science, and Technology. He was also a recipient of the 1996 EECS Department Teaching Excellence Award and a 2004 College of Engineering Research Excellence Award. In 2005 he received the IEEE GRSS Distinguished Achievement Award and the University of Michigan Faculty Recognition Award. He also received the best paper Award at the 2006 Army Science Conference. In 2008 he was awarded a Humboldt Research Award from The Alexander von Humboldt Foundation of Germany and received the best paper award at the IEEE Geoscience and Remote Sensing Symposium. He was also awarded the 2010 Distinguished Faculty Achievement Award from the University of Michigan. The IEEE Board of Directors announced him as the recipient of the 2011 IEEE Judith A. Resnik medal. In the past several years, joint papers presented by his students at a number of international symposia (IEEE APS'95,'97,'00,'01,'03,'05,'06,'07; IEEE IGARSS'99,'02,'07;'11 IEEE IMS'01, USNC URSI'04,'05,'06,'10,'11 AMTA'06, URSI GA 2008) have received best paper awards.

Authorized licensed use limited to: Seoul National University. Downloaded on December 15,2022 at 13:59:12 UTC from IEEE Xplore. Restrictions apply.